Neuronal defects and posterior pituitary hypoplasia in mice lacking the receptor tyrosine phosphatase PTPσ

M.J. Wallace[1*], J. Batt[1*], C.A. Fladd[1*], J.T. Henderson[2], W. Skarnes[3] & D. Rotin[1]

[*]*These authors contributed equally to this work.*

The LAR-family protein tyrosine phosphatase σ (PTPσ, encoded by the gene *Ptprs*) consists of a cell adhesion-like extracellular domain composed of immunoglobulin and fibronectin type-III repeats, a single transmembrane domain and two intracellular catalytic domains[1,2]. It was previously shown to be expressed in neuronal and lung epithelial tissues in a developmentally regulated manner[2–8]. To study the role of PTPσ in mouse development, we inactivated *Ptprs* by gene targeting. All *Ptprs*$^{+/-}$ mice developed normally, whereas 60% of *Ptprs*$^{-/-}$ mice died within 48 hours after birth. The surviving *Ptprs*$^{-/-}$ mice demonstrated stunted growth, developmental delays and severe neurological defects including spastic movements, tremor, ataxic gait, abnormal limb flexion and defective proprioception. Histopathology of brain sections revealed reduction and hypocellularity of the posterior pituitary of *Ptprs*$^{-/-}$ mice, as well as a reduction of approximately 50–75% in the number of choline acetyl transferase-positive cells in the forebrain. Moreover, peripheral nerve electrophysiological analysis revealed slower conduction velocity in *Ptprs*$^{-/-}$ mice relative to wild-type or heterozygous animals, associated with an increased proportion of slowly conducting, small-diameter myelinated fibres and relative hypomyelination. By approximately three weeks of age, most remaining *Ptprs*$^{-/-}$ mice died from a wasting syndrome with atrophic intestinal villi. These results suggest that PTPσ has a role in neuronal and epithelial development in mice.

We inactivated *Ptprs* gene targeting by inserting a cassette into an intron (interrupting the coding sequence between nt 460–850; ref. 1) in the first 1–2 immunoglobulin (Ig) repeats (Fig. 1*a*,*b*), which led to a complete absence of *Ptprs* message (Fig. 1*c*) and protein (Fig. 1*d*). This resulted in the gene encoding β-gal being fused to the upstream coding sequence of *Ptprs*, allowing us to analyse *Ptprs* expression during development in *Ptprs*$^{+/-}$ mice using lacZ staining. Our results show *Ptprs* expression from embryonic day (E) 14 to postnatal day (P) 1 in tissues of neuronal and epithelial origin, including hindbrain, developing cortex, hippocampus, cerebellum, cranial ganglia in the brainstem, pituitary gland, spinal cord (especially the dorsal root ganglia, DRG), lung and skin, but not in heart. By four weeks postnatal, expression was reduced and appeared restricted to hippocampal pyramidal neurons (data not shown). This pattern of expression is consistent with previous reports employing *in situ* hybridization[2–8].

Ptprs$^{+/-}$ mice were indistinguishable from wild-type mice, but *Ptprs*$^{-/-}$ mice, which constituted 19% (n=445 mice) of newborns, a likely underestimate, showed neuronal and epithelial defects. Most *Ptprs*$^{-/-}$ animals (59%) died immediately after birth. Those remaining (41%) showed growth retardation and neurological defects, and most died by three weeks of age from a wasting syndrome. The *Ptprs*$^{-/-}$ mice surviving to adulthood (11/445; 2.5%) were still approximately 50% smaller by weight than their wild-type or

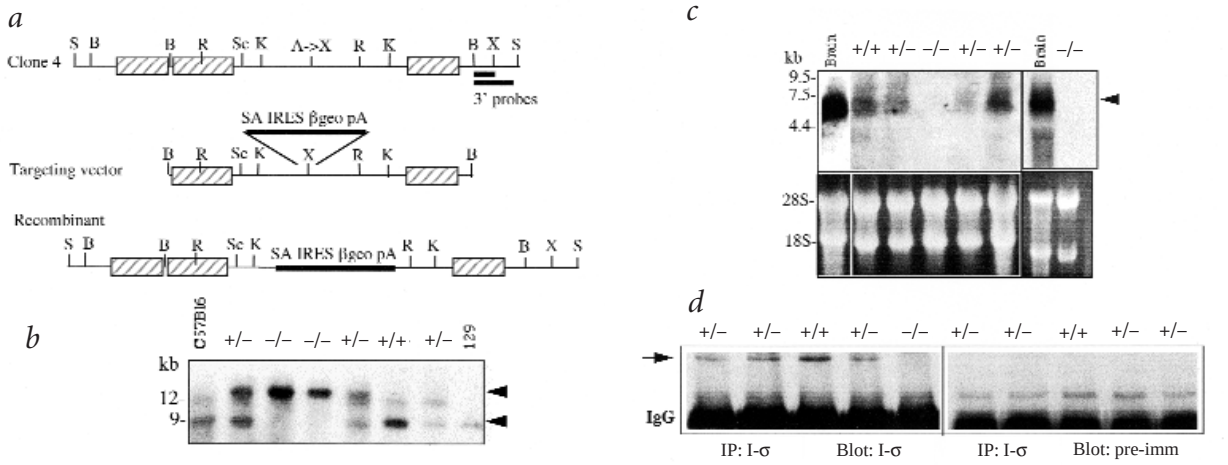

Fig. 1 Generation of *Ptprs*$^{-/-}$ mice. ***a***, Restriction map of *Ptprs* genomic clone 4 and the vector inserted into an *Xho*I site (generated from an *Aat*II site), interrupting the coding sequence between nt 460–850 (ref. 1) in the first 1–2 Ig repeats. ***b***, Genotyping of mice using tail DNA and Southern-blot analysis with the short 3′ probe shown in (*a*). C57Bl6 and 129 represent control DNA extracted from C57Bl6 mice and 129 genomic DNA. Arrows represent the 9.4- and 14-kb fragments corresponding to wild-type and *Ptprs*$^{-}$ alleles, respectively. ***c***, Analysis of expression of *Ptprs* in wild-type, *Ptprs*$^{+/-}$ and *Ptprs*$^{-/-}$ one-day-old mice using northern-blot analysis with a cDNA probe from rat *Ptprs* (95% identical to mouse *Ptprs* cDNA in that region) encompassing most of the extracellular domain (nt 796–3,760, excluding 1,086 nt corresponding to the spliced-out FNIII repeats, of rat *Ptprs*; ref. 1). Expression of *Ptprs* in adult rat brain is shown as a control. ***d***, Immunoprecipitation and subsequent immunoblotting with affinity purified anti-PTPσ (I-σ) antibody, directed against the intracellular juxtamembrane region of PTPσ. The antibody recognizes a 85-kD band (arrow) representing the proteolytically cleaved intracellular domain (and a short segment of the ectodomain) of PTPσ (left). The blot was stripped and reprobed with the pre-immune serum (Pre-imm) of the I-σ antibody (right). +/+, wild type; +/–, *Ptprs*$^{+/-}$; –/–, *Ptprs*$^{-/-}$; A, *Aat*II; B, *Bam*HI; K, *Kpn*I; R, *Eco*RI; S, *Sal*I; Sc, *Sac*I; X, *Xho*I; SA, splice acceptor; IRES, internal ribosome entry site; βgeo, lacZ (βgal) fused in frame to the neo gene; pA, poly(A); hatched bars, exons.

[1]*The Hospital for Sick Children, Programmes in Cell and Lung Biology, 555 University Avenue, Toronto, Ontario, M5G 1X8; and Biochemistry Department, University of Toronto, Toronto, Canada.* [2]*Samuel Lunenfeld Research Institute, Mt Sinai Hospital, 600 University Avenue, Toronto, Canada.* [3]*University of California at Berkeley, Department of Molecular and Cell Biology, 589 Life Science Addition, Berkeley, California 94720-3200, USA. Correspondence should be addressed to D.R. (e-mail:drotin@sickkids.on.ca).*

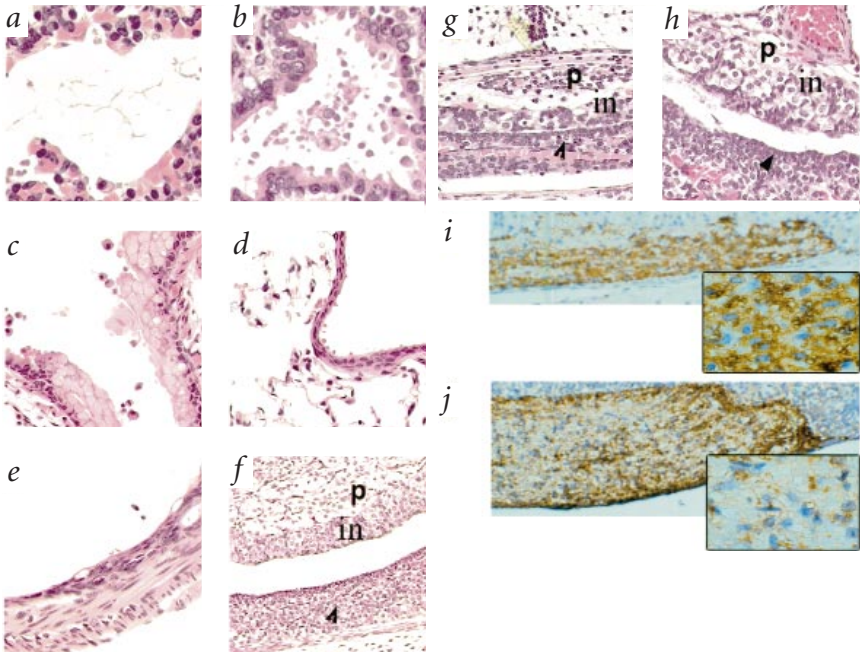

Fig. 2 Histopathology of lung, intestine and pituitary gland of *Ptprs*$^{-/-}$ mice. Lung sections show accumulation of granular fluid in lung airspaces (***a***), apical hypertension and blebbing of respiratory epithelial cells in the alveoli/airways of newborn *Ptprs*$^{-/-}$ mice (***b***; ×400 magnification), and microvesicular vacuolation and possible metaplasia of airway epithelial cells lining larger airways (***c***) of an 18-day-old *Ptprs*$^{-/-}$ mouse, compared with a similar airway from a wild-type mouse (***d***; ×400 magnification). ***e***, Large intestine showing flattening and atrophy of cells lining the intestine of a 16-day-old *Ptprs*$^{-/-}$ mouse (×400). ***f***, Normal pituitary gland from a one-day-old *Ptprs*$^{+/-}$ mouse showing relative size of the anterior pituitary (arrowhead), intermediate pituitary (in) and the overlying posterior (p) lobe. A cleft separates the anterior from the intermediate lobes (×100 magnification). Pituitary glands are shown from *Ptprs*$^{-/-}$ mice obtained from one-day-old (***g***) and newborn mice that died within hours after birth (***h***), demonstrating normal anterior (arrowhead) and intermediate (in) lobes adjacent to the cleft, but hypoplastic (*g*) or almost absent (*h*) posterior (p) lobes. (magnification ×200). Immunostaining with anti-oxytocin antibodies of *Ptprs*$^{+/-}$ (***i***) and *Ptprs*$^{-/-}$ (***j***) pituitary glands (magnification ×250) from three-week-old animals revealed reduced amounts of oxytocin in central regions in the posterior pituitary of *Ptprs*$^{-/-}$ relative to *Ptprs*$^{+/-}$ mice (insets; magnification ×1,000). Relative size differences between *Ptprs*$^{-/-}$ and *Ptprs*$^{+/-}$ posterior pituitaries in (*i–j*) are due to different positions within the gland during sectioning.

Ptprs$^{+/-}$ littermates, but were fertile. The phenotype of *Ptprs*$^{-/-}$ mice in the C57Bl6/129 background described here was similar to that seen in outbred CD1 background.

We next examined the pathology of *Ptprs*$^{-/-}$ mice of different ages. There was a reduction and hypocellularity of the posterior lobe of the pituitary gland in many *Ptprs*$^{-/-}$ mice examined. The anterior and intermediate lobes appeared normal. The posterior pituitary, which is neuronally derived, is normally rich in capillaries and populated by nerve fibers and neuroglial cells responsible for the production of oxytocin and vasopressin, but in *Ptprs*$^{-/-}$ animals it was characterized by poor cellularity, vacuolation and in some cases small size (Fig. 2*f–h*). Oxytocin immunostaining of the posterior lobe revealed a central pallor with dense granular staining of the periphery in five 2–3-week-old *Ptprs*$^{-/-}$ mice, which contrasted with the uniform dense staining in the posterior lobe of *Ptprs*$^{+/-}$ animals (Fig. 2*i,j*). This reduced central staining may be secondary to abnormal development and axon projection from the supraoptic and paraventricular nuclei, resulting in less dense innervation of the posterior pituitary.

Examination of major organs of *Ptprs*$^{-/-}$ mice that died immediately after birth revealed normal heart and kidney, but occasionally congested lungs with the accumulation of a granular fluid in the alveolar spaces (Fig. 2*a,b*), possibly representing surfactant and edema. Immaturity of the lung due to developmental delay[9,10] as well as abnormalities in the airway and alveolar epithelium resulting in defects in septal integrity and lung water clearance may have contributed to these findings.

Ptprs$^{-/-}$ mice surviving past 48 hours were smaller in size (Fig. 3*a*) and showed retarded development, including overall growth, a one-day delay in body hair growth and two-day delay in eyelid opening. Most of these mice died by 2–3 weeks of age. Histopathology analysis of the gastrointestinal (GI) tract of these animals revealed atrophy and blunted villi in the intestine and colon (Fig. 2*e*). There was also occasional obstruction or blockage of the colon. These features may result from lack of trophic factors during development, impaired nutrition or secondary colonic obstruction from reduced gut motility. We observed reduced numbers of autonomic ganglia surrounding the intestinal muscles, in support of possible diminished gut motility. Our

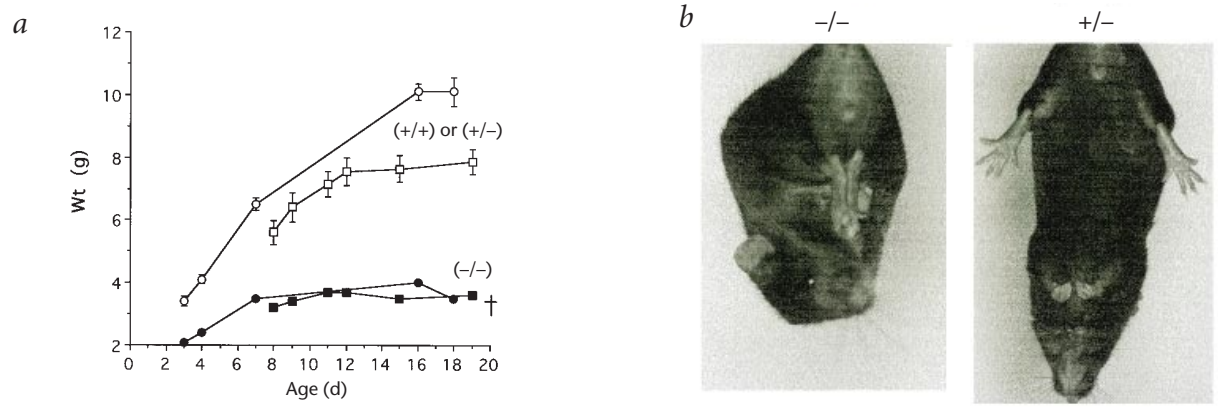

Fig. 3 Growth retardation and abnormal limb flexion in *Ptprs*$^{-/-}$ mice. ***a***, Weight gain of *Ptprs*$^{-/-}$ mice relative to wild-type and *Ptprs*$^{+/-}$ littermates. Two litters are represented containing four or eight mice. Each litter has one *Ptprs*$^{-/-}$ mouse, which died at the indicated age (†). ***b***, Abnormal limb flexion of *Ptprs*$^{-/-}$ mice, demonstrating 'clutching' of a *Ptprs*$^{-/-}$ mouse (left) relative to a normal littermate (right) when suspended by the tail. All *Ptprs*$^{-/-}$ mice, regardless of age, showed this phenotype.

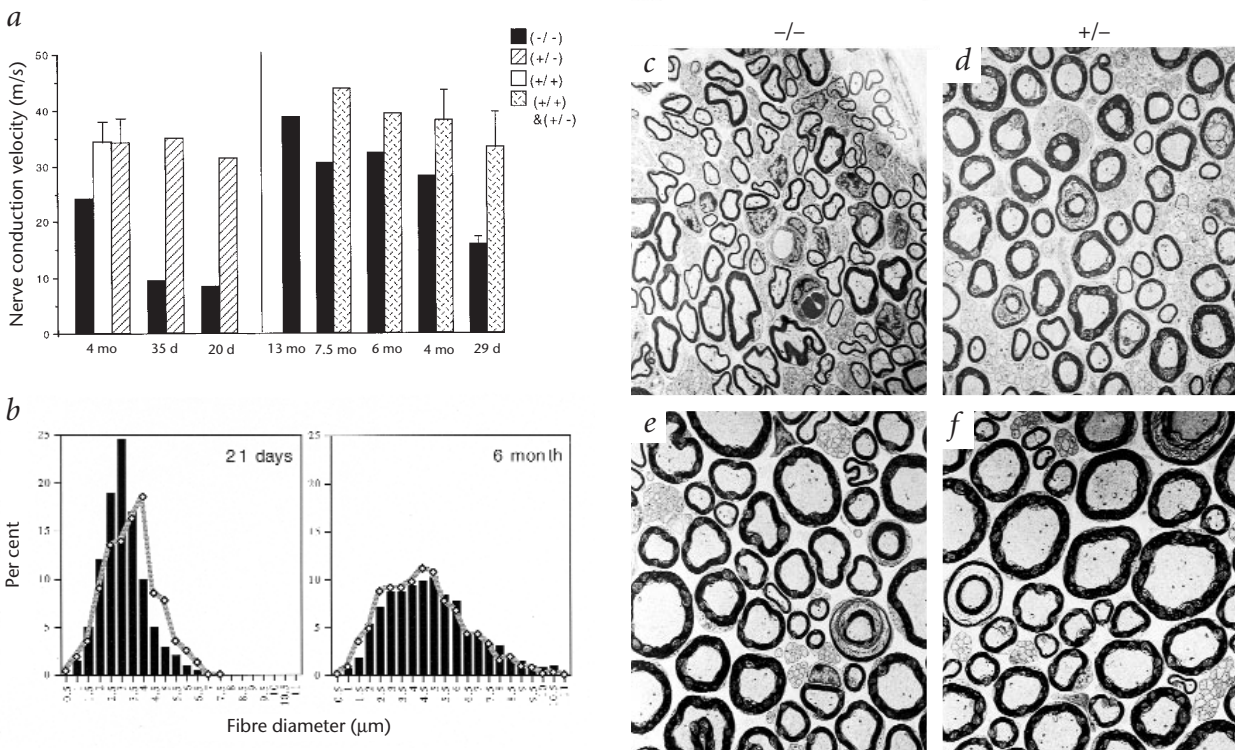

Fig. 4 Abnormal peripheral nerve conduction velocity and myelinated fibre size. ***a***, Peripheral nerve motor conduction velocity. Left, motor nerve conduction velocities (NCV) in adult 4-month (mo), 35- and 20-day mice were calculated from the action potential generated by stimulating the proximal sciatic nerve and recording in the gastrocnemius[22]. For wild-type and *Ptprs*$^{+/-}$ adults, values represent the mean±s.e. of 10–13 measurements from 5–6 animals. For *Ptprs*$^{-/-}$ 35-d and *Ptprs*$^{+/-}$ 20-d mice, data represent the average of two measurements (right and left legs) from one animal in each age group. Right, intersegmental motor NCV in adult 4–13-month and 29-d mice were calculated from the action potential generated by proximally stimulating the sciatic nerve, distally stimulating the posterior tibial nerve and recording in the adductor hallucis brevis muscle[21]. Values represent the mean±s.d. of five measurements from five *Ptprs*$^{+/-}$ adult 4-month mice, and the average of two measurements (right and left legs) of each adult *Ptprs*$^{-/-}$ 6-month and *Ptprs*$^{-/-}$ 7.5-month mice. For the day 29 animals, values represent the mean±s.d. of measurements from five wild-type or *Ptprs*$^{+/-}$ mice, or mean±s.d. of five measurements from three *Ptprs*$^{-/-}$ mice. ***b***, Sciatic nerve myelinated-fibre diameter histogram (at the level of trifurcation). Representative histograms from day 21 *Ptprs*$^{-/-}$ (black bars) and *Ptprs*$^{+/-}$ (grey line) mice demonstrate unimodal distribution of fibre diameter compatible with a young developing nerve[27,28]. *Ptprs*$^{-/-}$ animals show a left shift towards a greater proportion of small-diameter fibres compared with sibling controls, suggesting developmental delays. Histograms obtained from adult (6 month) *Ptprs*$^{-/-}$ or *Ptprs*$^{+/-}$ mice demonstrate the larger absolute myelinated-fibre diameters and broader range classic of a mature nerve. These histograms overlap, revealing near resolution of *Ptprs*$^{-/-}$ developmental delay at this age. Histograms represent measurements of more than 500 myelinated fibres performed on three *Ptprs*$^{-/-}$ and three *Ptprs*$^{+/-}$ animals (a typical representative of each depicted here). *c–f*, Corresponding EM analyses of the sciatic nerve at the level of trifurcation (×5,360 magnification). Electron micrographs of 21-d *Ptprs*$^{-/-}$ or *Ptprs*$^{+/-}$ mice (***c***,***d***) depict the larger proportion of small diameter fibres in *Ptprs*$^{-/-}$ nerve and increased axon/myelin area ratio. EM of the adult (Ad) nerves (***e***,***f***) reveal larger fibre diameters and myelin thickening in both *Ptprs*$^{-/-}$ and *Ptprs*$^{+/-}$ animals.

observations point to defects in epithelial development resulting from the absence of PTPσ expression.

We performed neurobehavioural, electrophysiology, immunohistochemical and electron microscopy assessments to analyse the neuronal defects in *Ptprs*$^{-/-}$ mice. Mice surviving past 48 hours showed signs of neurological abnormalities, including fine intention tremor most pronounced in hindquarter and tail, ataxic gait and spasticity that was most notable in the hindquarter. In mice surviving to adulthood, these characteristics resolved with age, suggesting they are secondary to delayed neurologic development. When normal mice are suspended by the tail, they extend their legs (Fig. 3*b*, right), but *Ptprs*$^{-/-}$ mice reflexively contract their limbs (Fig. 3*b*, left); this abnormal limb flexion was not corrected with age. This reflex was observed in 100% (34/34) of *Ptprs*$^{-/-}$ mice and was similar to that described for NF-H overexpressing mice[11]. Several of these neuronal abnormalities, including the fine intention tremor, abnormal limb flexion and ataxic gait, are consistent with cerebellar defects. So far no gross abnormalities in the cerebellum of *Ptprs*$^{-/-}$ mice have been detected, although PTPσ is normally expressed in this region during early postnatal life, suggesting it may have a role in some aspects of cerebellar function.

A series of neurobehavioural tests performed on the mice revealed that although there was no difference in behaviour between wild-type and heterozygous mice, *Ptprs*$^{-/-}$ mice, regardless of age, demonstrated abnormal acceleration righting (34/34) and proprioception (3/3). These responses were permanent and did not correct with maturation. We speculate that the proprioceptive defects may be the result of inadequate PTPσ expression in the DRG or cerebellum. Other tests, including the righting response, geotaxic response and bar grip, that young *Ptprs*$^{-/-}$ mice failed, were corrected with age, suggesting developmental delays may be responsible.

To assess peripheral nerve function, we determined motor nerve conduction velocities (NCV) for the sciatic and posterior tibial nerves using two minimally invasive percutaneous electrophysiologic methodologies. There was no difference in NCV between adult wild-type and *Ptprs*$^{+/-}$ mice, whereas it was reduced in age-matched adult *Ptprs*$^{-/-}$ mice (Fig. 4*a*). Moreover, this reduction was more pronounced in the less mature, 20-, 29- or 35-day-old *Ptprs*$^{-/-}$ animals. Average NCV of young wild-type and *Ptprs*$^{+/-}$ 29-day mice was slightly slower than that of their adult counterparts (Fig. 4*a*, right), consistent with known maturation changes in motor NCV. Increasing velocity occurs in the normal developing mammalian nerve secondary to a number of factors, including an increase in the proportion of fast-conducting, large-diameter fibres and an increase in myelin thickness. *Ptprs*$^{-/-}$ mice also demonstrated increasing velocities with age, but did not reach the speed of

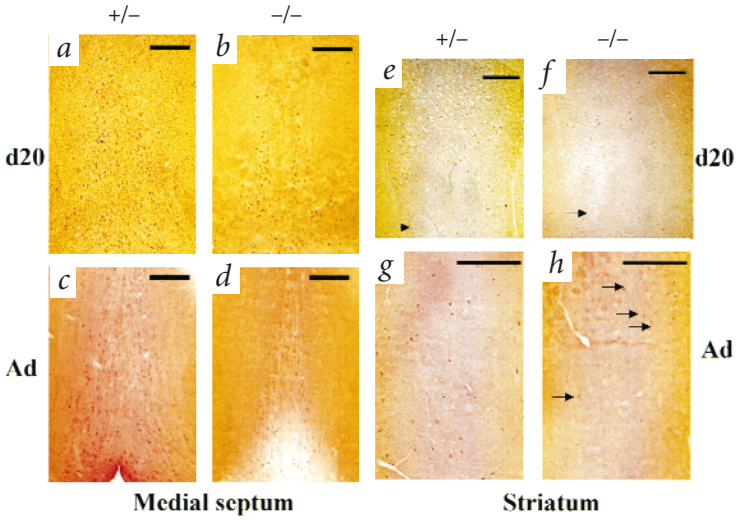

Fig. 5 Reduction in numbers of cholinergic neurons in the forebrain analysed by ChAT staining. ChAT staining of coronal sections within the medial septum (*a*–*d*) and striatum (*e*–*h*) of 20-d mice (***a***,***b***,***e***,***f***) or 6-month (Ad) mice (***c***,***d***,***g***,***h***). There was a reduction of approximately 50% in the number of ChAT-positive neurons in striatum and medial septum of the 20-d *Ptprs*$^{-/-}$ mice and in medial septum of both 20-d and adult *Ptprs*$^{-/-}$ mice relative to *Ptprs*$^{+/-}$ controls. The reduction in ChAT staining in the medial septum of adult *Ptprs*$^{-/-}$ mice was even greater (~75%) relative to *Ptprs*$^{+/-}$ controls. For all these analyses, serial coronal sections, taken at 150-μm intervals, were analysed for ChAT staining, and representative sections taken at equivalent coronal levels. Arrows in (*e*,*f*) indicate the relative position of the pars anterior of the anterior commissure. Arrows in (*h*) mark the few ChAT-positive neurons present in the striatum of *Ptprs*$^{-/-}$ mice. Scale bar, 200 μm.

a mature nerve until one year of age, nine months behind their wild-type and *Ptprs*$^{+/-}$ counterparts. Histologic analysis suggested the decreased velocities were, in part, secondary to developmental delay. Electron microscopy and morphometric analysis revealed a significantly increased proportion of slowly conducting, small-diameter myelinated fibres in *Ptprs*$^{-/-}$ compared with young *Ptprs*$^{+/-}$ animals (Fig. 4*b*–*f*). Average axon area and myelin area ratios were also significantly larger in young *Ptprs*$^{-/-}$ (0.724) compared with *Ptprs*$^{+/-}$ (0.619) mice, suggesting relative hypomyelination in the former. Analysis of six-month-old animals revealed development of the nerves to maturity with a significant increase in the range and absolute value of myelinated fibre diameter and myelin thickness, which was identical in *Ptprs*$^{-/-}$ and *Ptprs*$^{+/-}$ animals. Both DRG and spinal motor neurons, which send axonal projections to the sciatic nerve, express high levels of PTPσ during synaptogenesis[8]. Thus, the developmental delay seen in the sciatic nerve of *Ptprs*$^{-/-}$ mice may be directly related to the absence of PTPσ in these cells. In addition, this finding is consistent with the failure of neurobehavioural testing involving power by young *Ptprs*$^{-/-}$ animals (that is, bar grip, geotaxic response and righting reflex, and subsequent correction with age.

Histopathology and immunohistochemistry analyses of the CNS revealed no gross abnormalities in the overall brain structure of *Ptprs*$^{-/-}$ mice, except for the expected smaller size. Staining for specific subsets of interneurons using calretinin, parvalbumin and calbindin D-28 throughout the CNS revealed no difference (data not shown). ChAT immunostaining, however, which marks choline acetyl transferase-positive cells, revealed a reduction of approximately 50–75% in the number of cholinergic neurons in the forebrain of both young (0–3 weeks) and mature (6 months) *Ptprs*$^{-/-}$ animals that was most prominent in the medial septum and striatum (Fig. 5). In contrast, this reduction was not observed in other cholinergic sites, such as the facial and hypoglossal nuclei of the brainstem (data not shown).

PTPσ has previously been shown to be expressed in the central and peripheral nervous system, as well as in lung epithelia, in a developmentally regulated fashion[2–8]. Adhesion molecules expressed at the surface of neurons, including those belonging to the immunoglobulin superfamily such as NCAM, fasciclin II and L1, are known to be involved in axon growth and guidance. LAR, PTPσ and PTPδ possess extracellular domains composed of immunoglobulin type C2 and FNIII repeats and thus belong to the same superfamily. The *Drosophila* homologue of LAR/PTPσ/PTPδ, DLAR, as well the related DPTP69D, are expressed in CNS axons and implicated in axon pathfinding and motoneuron guidance[12,13]. The axonal routing defect seen in one *Ptprs*$^{-/-}$ mouse in which crossing of the corpus callosum was impaired (data not shown), as well as potential impaired axonal projection in the posterior pituitary, are in support of the role PTPσ has in neuronal development and pathfinding, as seen in *Drosophila*.

Mice mutant for LAR (refs 14,15) are viable, have a normal lifespan and reproduce, but do show defects in branching morphogenesis of the mammary glands[15] and a reduction in number of cholinergic neurons in the forebrain[16] (medial septum), similar to *Ptprs*$^{-/-}$ mice. So far, however, no neurologic phenotype has been reported in LAR-mutant mice. An impaired mammary development was also noted in *Ptprs*$^{-/-}$ mothers (data not shown). Gene targeting of the active catalytic site of PTPδ (N. Vetani *et al.*, pers. comm.) led to the generation of mutant mice that share several common features with *Ptprs*$^{-/-}$ mice, including growth retardation, abnormal positioning of hindlimbs and abnormal limb flexing. In some regions of the CNS (for example, hippocampus and pituitary gland), both PTPσ and PTPδ are expressed during similar periods of development[6,17], suggesting co-expression, and we have recently demonstrated an association between PTPσ and PTPδ via their catalytic domains, suggesting that these two closely related phosphatases heterodimerize[18]. In view of some overlapping phenotypes of the mice lacking either of these two functional proteins, it is possible that these two PTPs operate in concert, and that removal of either one is sufficient to cause some of the neuronal defects seen in *Ptprs*$^{-/-}$ mice.

Methods

***Ptprs* inactivation.** Mouse 129 genomic library was probed with a rat *Ptprs* 5′ 462-bp fragment encoding the signal peptide, ATG and part of the first Ig domain. The genomic clone isolated (clone 4) included a 9.4-kb *Bam*H1 fragment, which contained at least two exons separated by a large intron. This *Bam*H1 fragment was subcloned into pUC19, and the gene-targeting cassette was inserted into an *Xho*I site (altered from an *Aat*II site) in an intron within this fragment. The targeting cassette consists of a splice acceptor (SA), an internal ribosome entry site (IRES), lacZ fused to neo (βgeo) and a poly(A) sequence. The resulting protein should consist of no more than the first 1–2 Ig repeats of PTPσ followed by lacZ and neo. We electrporated the vector into ES cells (CJR8.8, strain 129) and verified incorporation of the allele following homologous recombination by the presence of an approximately 14-kb *Hin*dIII fragment (in addition to the native 9-kb fragment) in Southern-blot analysis using a *Bam*H1-*Sal*I 3′ probe. Clone 7 was then mated to generate heterozygous offspring and backcrossed (that is, *Ptprs*$^{+/-}$×C57Bl6 mice) to purify the line. Southern-blot analysis of tail genomic DNA using a 650-bp *Bam*HI-*Xho*I 3′ probe was then used to identify wild-type, *Ptprs*$^{+/-}$ and *Ptprs*$^{-/-}$ mice, as performed above for the ES cells. To assess expression of *Ptprs*, northern-blot analysis was performed on head total RNA using a 1.8-kb fragment (nt 796–3,760 of rat *Ptprs* cDNA, 95% nucleotide identity to mouse *Ptprs*) as a probe[1], which encompasses most of the extracellular domains, excluding the 1,086 nt corresponding to the spliced FNIII repeats not present in the major brain form (~6.5 kb) of PTPσ. The expected 6.5 kb (or 7.5 kb) transcripts were not present in

Ptprs$^{-/-}$ mice. Accordingly, immunoprecipitation followed by western-blot analysis of newborn brain lysates using an affinity-pure anti-peptide antibody (I-σ), directed against the unique sequence KPDSKRKDSEPRTKCLL present at the intracellular juxtamembrane region of PTPσ (aa 1,240–1,256; ref. 1), revealed the presence of the expected 85-kD band in wild-type and *Ptprs*$^{+/-}$ mice, but not in *Ptprs*$^{-/-}$ animals.

Histology and immunohistochemistry. Tissues were fixed in 4% paraformaldehyde, sectioned (5 μm) and stained with haematoxylin and eosin. For cryostat sections following fixation, we washed samples in PBS and placed them in 30% sucrose in 0.1% PBS solution overnight at 4 °C. Tissue samples were then frozen and cut at 30-μm intervals on a cryostat. For neuronal staining of brain sections, cryostat coronal sections were taken at 150-μm intervals through the entire brain. Sections were blocked and incubated with primary antibodies to either choline acetyl transferase (ChAT), calretinin (Chemicon), parvalbumin or calbindin D 28K (Sigma), followed by biotinylated secondary antibodies (Vector Labs) and Streptavidin-HRP (Vectastain ABC kit) and developed in 0.05% DAB/0.03% H_2O_2 solution, as described[19]. For immunostaining of the posterior pituitary, tissue was fixed in 4% paraformaldehyde and 0.2% glutaraldehyde for 24 h at 4 °C, washed twice overnight in PBS, transferred to 70% ethanol and paraffin embedded. Pituitary sections (5 μm) were rehydrated through a standard gradient of alcohol washes. Sections were incubated with primary antibody against oxytocin (Sigma), followed by biotinylated secondary antibody and Streptavidin-HRP (Vectastain Elite ABC Kit, Vector Labs) and developed in DAB (0.6 mg/ml) and H_20_2 (0.03%). For electron microscopy, the sciatic nerve was dissected from the sciatic notch down to and including the muscular insertion of its major branches (posterior tibial, peroneal and sural) in the posterior calf. Nerve tissue was fixed in 2.5% glutaraldehyde, sodium cocodylate buffer (0.025 M), washed in sodium cocodylate buffer (0.05 M) followed by water and post-fixed in 2% osmium tetroxide. Dehydration was carried out in graded acetone, followed by embedding in Epon. Sections (1 μm) were stained with toluidine blue and ultrathin sections were stained with uranyl acetate and lead citrate. Electron microscopic examination was performed with a Phillips 201 (N.V. Philips) transmission electron microscope. For LacZ staining, tissues were dissected from *Ptprs*$^{+/-}$ mice (or wild-type controls) of day 14 fetuses, day 1 postnatal and adult mice and fixed in 0.2% gluteraldehyde solution as described[20] and stained with X-gal in potassium ferro/ferri-cyanide (5 mM; Sigma) solution. Nerve morphology was determined from toluidene blue-stained sections of the sciatic nerve at the level of the trifurcation (×1,000 magnification). The microscopic image was digitized and analysed based on a gray/white scale by morphometry software (Leco Instruments). For each nerve segment, we measured total fascicular area and evaluated a minimum of 500 myelinated axons for the area and diameter of axon, myelin and fibre. Fibre-diameter histograms were derived from these primary measurements.

Electrophysiological analysis. Peripheral nerve conduction velocity in anesthaetized mice was determined for the sciatic and posterior tibial peripheral nerves as described[21,22]. Recording electrodes were percutaneously placed in the adductor hallucis brevis muscle. Stimulating electrodes were percutaneously inserted into the sciatic nerve at the level of the sciatic notch for proximal stimulation, and in the posterior tibial nerve at the medial malleolus for distal stimulation. A 0.05-ms square wave stimulus, at two times threshold level, was delivered with a Neuromax Stimulator (Excel) to the proximal sciatic nerve. The latency, amplitude and area of resultant action potential were recorded. Distal stimulation at the medial malleolus was then performed. NCV in the intervening segment of the sciatic and posterior tibial nerves was calculated via standard formula[21]. In animals in which only one site of stimulation was available, the recording electrode was placed in the gastrocnemius and the NCV was determined as described[22].

Neurobehavioural assessment. Neurobehavioural tests performed[23–26] were: (i) righting reflex, the ability of mice to right themselves immediately following placement on their backs; (ii) acceleration righting, the ability to land on four feet following a 10-cm drop (on a soft surface) of mice held by their tails; (iii) geotaxic response, the ability to turn around and walk up a 45° incline following placement, head downward, on the incline; (iv) bar grip, the ability to grasp a bar with all four feet and curl the tail around it; (vi) proprioception, the animal was supported so that one forelimb was resting on a flat surface, then gentle pressure was applied to the medial aspect of the forelimb (the normal response is to lift the foot and replace it, hopping across the surface laterally as ongoing pressure is applied); and (vii) walking on a flat surface, the ability to walk on a smooth, flat surface.

Acknowledgements

We thank C. McKerlie for histopathology analyses; J. Bain for assistance with nerve conduction analyses; B. Goldstein for Ptprs cDNA; J. Rossant for 129 genomic DNA library; and D. Hunter for assistance with the peripheral nerve morphometric analysis. This work was supported by a Group Grant in Lung Development from the Medical Research Council (MRC) of Canada (to D.R.). D.R. was a recipient of an MRC Scholarship. M.J.W. was supported by Canadian Lung Association/MRC Fellowships. J.B. is a recipient of an MRC Fellowship.

Received 4 August 1998; accepted 4 February 1999.

1. Zhang, W.-R., Hashimoto, H., Ahmad, F., Ding, W. & Goldstein, B.J. Molecular cloning and expression of a unique receptor-like protein tyrosine phosphatase in the leukocyte-common-antigen-related phosphatase family. *Biochem. J.* **302**, 39–47 (1994).
2. Yan, H. *et al.* A novel receptor tyrosine phosphatase-σ that is highly expressed in the nervous system. *J. Biol. Chem.* **268**, 24880–24886 (1993).
3. Sahin, M. & Hockfield, M. Protein tyrosine phosphatases expressed in the developing rat brain. *J. Neurosci.* **13**, 4968–4978 (1993).
4. Walton, K.M., Martell, K.J., Kwak, S.P., Dixon, J.E. & Largent, B.L. A novel receptor-type protein tyrosine phosphatase is expressed during neurogenesis in the olfactory neuroepithelium. *Neuron* **11**, 387–400 (1993).
5. Stoker, A.W., Gehring, B., Haj, F. & Bay, B.H. Axonal localisation of the CAM-like tyrosine phosphatase CRYPα: a signalling molecule of embryonic growth cones. *Development.***121**, 1833–1844 (1995).
6. Wang, H. *et al*. Expression of receptor protein tyrosine phosphatase-σ (RPTP-σ) in the nervous system of the developing and adult rat. *J. Neurosci. Res.* **41**, 297–310 (1995).
7. Kim, H. *et al*. Expression of LAR-PTP2 in rat lung is confined to proliferating epithelia lining the airways and air sacs. *Am. J. Physiol.* **14**, L566–576 (1996).
8. Haworth, K., Shu, K.K., Stokes, A., Morris, R. & Stokes, A. The expression of receptor tyrosine phosphatases is responsive to sciatic nerve crush. *Mol. Cell. Neurosci.* **12**, 93–104 (1998).
9. Bourbon, J.R. & Fraslon, C. Developmental aspects of the alveolar epithelium and pulmonary surfactant system. in *Pulmonary Surfactant: Biochemical, Functional, Regulatory and Clinical Concepts* (ed. Bourbon, J.R.) 257–324 (CRC Press, New York, 1996).
10. Pitkanen, O. & O'Brodovich, H. Significance of ion transport during lung development and in respiratory disease of the newborn. *Ann. Med.* **30**, 134–142 (1997).
11. Côté, F., Collard, J.-F. & Julien, J.-P. Progressive neuropathy in transgenic mice expressing the human neurofilament heavy gene: a mouse model for amyotrophic lateral sclerosis. *Cell* **73**, 35–46 (1993).
12. Desai, C.J., Gindhart, J.G. Jr, Goldstein, L.S.B. & Zinn, K. Receptor tyrosine phosphatases are required for motor axon guidance in the *Drosophila* embryo. *Cell* **84**, 599–609 (1996).
13. Krueger, N.X. *et al*. The transmembrane tyrosine phosphatase DLAR controls motor axon guidance in Drosophila. *Cell* **84**, 611–622 (1996).
14. Skarnes, W.C., Moss, J.E., Hurtley, S.M. & Beddington, R. Capturing genes encoding membrane and secreted proteins important for mouse development. *Proc. Natl Acad. Sci. USA* **92**, 6592–6596 (1995).
15. Schaapveld, R.Q.J. *et al*. Impaired mammary gland development and function in mice lacking LAR receptor-like tyrosine phosphatase activity. *Dev. Biol.* **188**, 134–146 (1995).
16. Yeo, T.T. *et al*. Deficient LAR expression decreases basal forebrain cholinergic neuronal size and hippocampal cholinergic innervation. *J. Neurosci. Res.* **47**, 348–360 (1997).
17. Sommer, L., Rao, M. & Anderson, D.J. RPTPδ and the novel tyrosine phosphatase RPTPψ are expressed in restricted regions of the developing central nervous system. *Dev. Dyn.* **208**, 48–61 (1997).
18. Wallace, M.J., Fladd, C., Batt, J. & Rotin, D. The second catalytic domain of the protein tyrosine phosphatase δ (PTPδ) binds to and inhibits the first catalytic domain of PTPσ. *Mol. Cell. Biol.* **18**, 2608–2616 (1998).
19. Jacobowitz, D.M. & Abbott, L.C. *Chemoarchitectonic Atlas of the Developing Mouse Brain* (CRC, New York, 1997)
20. Henderson, J.T., Javaheri, M., Kopko, S. & Roder, J.C. Reduction of lower motor neuron disease in wobbler mice by N-acetyl-L-cysteine. *J. Neurosci.* **16**, 7574–7582 (1996).
21. Robertson, A., Day, B., Pollock, M. & Collier, P. The neuropathy of elderly mice. *Acta Neuropathol.* **86**, 163–171 (1993).
22. Smorto, M.P. & Basmajian, J.V. Introduction to nerve conduction tests. in *Clinical Electroneurography* 19–56 (Williams and Wilkins, Philadelphia, 1979).
23. Crawley, J.N. & Paylor, R. A proposed test battery and constellation of specific behavioral paradigms to investigate the behavioral phenotypes of transgenic and knockout mice. *Horm. Behav.* **31**, 197–211 (1997).
24. Rogers, D.C. *et al*. Behavioral and functional analysis of mouse phenotype: SHIRPA, a proposed protocol for comprehensive phenotype assessment. *Mamm. Gen.* **8**, 711–713 (1997).
25. Irwin, S. Comprehensive observational assessment: Ia. Systematic, quantitative procedure for assessing the behavioral and physiologic state of the mouse. *Psychopharmacologia* **13**, 222–257 (1968).
26. Oliver, J. & Lorenz, M. Neurologic examination. in *Handbook of Veterinary Neurological Disorders* 19–51 (W.B. Saunders, Orlando, 1983).
27. Ferriere, G., Denef J., Rodriguez, J. & Guzzetta, F. Morphometric studies of normal sural nerves in children. *Muscle Nerve* **8**, 697–704 (1985).
28. Ouvrier, R., McLeod, J.G. & Conchin, T. Morphometric studies of sural nerve in childhood. *Muscle Nerve* **10**, 47–53 (1987).